A Miniature 500 000-r/min Electrically Driven Turbocompressor

Daniel Krähenbühl, *Student Member, IEEE*, Christof Zwyssig, *Member, IEEE*, Hansjörg Weser, and Johann W. Kolar, *Fellow, IEEE*

***Abstract*—The trend in compressors for fuel cells, heat pumps, aerospace, and automotive heating, ventilation, and air-conditioning systems is toward ultracompact size and high efficiency. This can be achieved by using turbocompressors instead of scroll, lobe, or screw compressors, increasing the rotational speed and employing new electrical drive system technology and materials. This paper presents a miniature electrically driven two-stage turbocompressor system running at a rated speed of 500 000 r/min. The design includes the thermodynamic analysis, the electric motor, the inverter, the control, and the system integration with rotor dynamics and thermal considerations. Experimental measurements such as the compressor map are presented for air under laboratory conditions. The two-stage turbocompressor has been tested up to a speed of 600 000 r/min, where a maximal pressure ratio of 2.3 at a mass flow of 0.5 g/s has been reached. To the authors' knowledge, this is the highest rotational speed achieved with an electrically driven turbocompressor.**

***Index Terms*—Electric drives, permanent-magnet (PM) machines, turbocompressor, ultrahigh speed.**

I. Introduction

IN FUTURE CARS and airplanes, more and more hydraulic, pneumatic, and mechanical systems and compressors will be replaced with electrically driven systems; the trend is to more-electric aircraft and vehicles. Examples are the compressors for heating, ventilation, and air conditioning in cars or air pressurization for aircraft cabins. The power levels of these electrically driven compressors are from about 100 W up to a few kilowatts. Additionally, several car manufacturers have research projects or even prototypes on electric vehicles with fuel-cell propulsion systems or fuel-cell systems as a range extender. Moreover, in trucks and aircrafts, fuel cells are planned to be used as auxiliary power units. A manned aircraft with a fuel-cell/lithium-ion battery hybrid system to power an electric motor coupled to a conventional propeller successfully completed a flight in Spain [1]. At the Georgia Institute of Technology, unmanned fuel-cell-powered aerial vehicles have been designed and tested [2].

All these fuel cells usually need an electrically driven air compressor, which consumes around 10%–20% of the output power of the fuel cell, and the pressure ratios are usually between 1.5 and 2.5 [3]. The electrically driven air compressor should be small, lightweight, and efficient.

Other applications for electrically driven compressors are residential applications such as heat pumps in order to enable a more rational use of energy [4]. Moreover, there, the trend is to more-compact systems with a higher efficiency. Distributed heat pump systems could be realized with smaller compressors and expanders.

All of these applications need ultracompact highly efficient electrically driven compressor systems, and they have a strong link to renewable-energy systems. Turbocompressors have, both in size and efficiency, advantages over other compressor types, such as scroll, lobe, or screw compressors [3]. In both turbomachinery and electrical machines, power density increases with increasing the rotational speed [5], [6]. Therefore, these systems ideally have rotational speeds between 100 000 and 1 000 000 r/min at power levels of 100 W up to several kilowatts.

In this paper, a miniature two-stage electrically driven turbocompressor system is presented. It has a rated rotational speed of 500 000 r/min for a calculated air pressure ratio of 2.25 and a mass flow of 1 g/s at ambient conditions for temperature and inlet pressure. The system is designed for the cabin air pressurization system of the Solar Impulse airplane [7], but the specifications are in the area of the other applications mentioned. The design is based on a one-stage electrically driven compressor built as a first prototype [8]. The two-stage version of the compressor is required for an increase in pressure ratio. This is necessary because the maximum flying altitude will be around 12 000 m. The system is shown in Figs. 1 and 7; it is comprised of two radial impellers, a permanent-magnet (PM) motor, and the power and control electronics. The paper starts with the main scaling laws of turbomachinery, electrical machine, and power and control electronics, and then describes the different components, i.e., the electrical machine, the power electronics, and the turbomachinery, as well as the system integration including the thermal and rotordynamic design. Finally, measurement results are presented.

Manuscript received December 26, 2009; revised March 10, 2010; accepted April 28, 2010. Date of publication September 7, 2010; date of current version November 19, 2010. Paper 2009-IDC-486.R1, presented at the 2009 IEEE Energy Conversion Congress and Exposition, San Jose, CA, September20–24, and approved for publication in the IEEE TRANSACTIONS ON INDUSTRY APPLICATIONS by the Industrial Drives Committee of the IEEE Industry Applications Society.

D. Krähenbühl is with the Power Electronic System Laboratory, Swiss Federal Institute of Technology (ETH) Zurich, 8092 Zurich, Switzerland, and also with Celeroton Ltd., 8092 Zurich, Switzerland (e-mail: kraehenbuehl@lem.ee.ethz.ch).

C. Zwyssig is with Celeroton Ltd., 8092 Zurich, Switzerland (e-mail: christof.zwyssig@celeroton.com).

H. Weser is with High-Speed Turbomaschinen GmbH, 38165 Lehre, Germany (e-mail: h.weser@hsturbo.de).

J. W. Kolar is with the Power Electronic System Laboratory, Swiss Federal Institute of Technology (ETH) Zurich, 8092 Zurich, Switzerland (e-mail: kolar@lem.ee.ethz.ch).

Color versions of one or more of the figures in this paper are available online at http://ieeexplore.ieee.org.

Digital Object Identifier 10.1109/TIA.2010.2073673

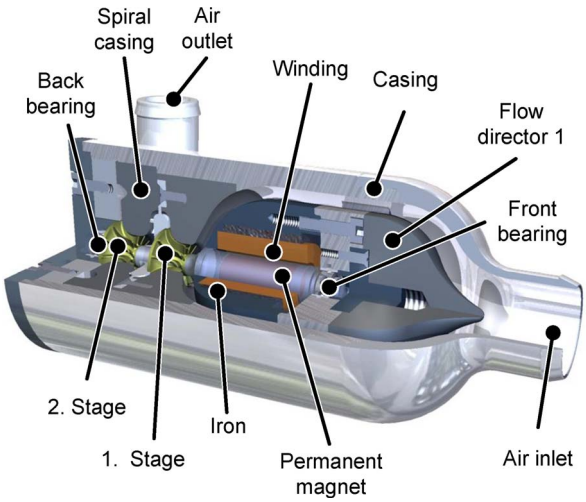

Fig. 1. Cross-sectional view of the integrated two-stage electrically driven turbocompressor system.

II. Scaling Laws

There are two reasons for downscaling the turbomachinery. First, in high-power applications, the power density can be increased with modularization, and second, new emerging applications demand compressors with lower mass flow at constant pressure ratios. In [5], it is shown that the power density (P/V) of the turbomachinery is inversely proportional to the rotor outlet diameter d_2 of the turbomachinery, i.e.,

$$\frac{P}{V} \propto \frac{1}{d_2}. \tag{1}$$

This implies that a conventional turbomachine with a certain output power can get replaced with a number of smaller units, which have, all together, the same total output power but a smaller overall volume. This scaling implies constant surface speed, which means that the rotational speed scales inversely proportional with diameter d_2, as shown in (6). However, this is not fully accurate, as a major condition for the scaling of the turbomachinery is a constant Reynolds number, which is also proportional to the dimension of the flow channel and the height of the airflow channel d_h, as shown in (2). Since the Reynolds number decreases with miniaturization and does not remain constant, the power density increases less than $1/d_2$. The Reynolds number can be calculated as

$$\mathrm{Re} = \frac{c d_h}{v} \tag{2}$$

where c is the speed of the fluid in the flow channel and v is the kinematic viscosity. As an example, one large turbocompressor can be replaced with 16 compressors, each with a volume of 1/64 of the conventional compressor, which together has the same output power but requires only a quarter of the volume of the conventional compressor. The diameter of the small units would be 1/4 of the original one, and the rotational speed would therefore increase by a factor of at least 4. This scaling is only true under the assumption that only the active parts of the turbomachinery and the electrical machines are taken into account but not the inactive parts, such as the housing of the turbomachinery and the electrical machine, the power electronics, and airflow channels for cooling. For the system presented in this paper, the total volume (inlet junction neglected) is 48 cm^3, thereof the electrical machine has a volume of 3.2 cm^3, and the two compressor stages have a volume of 6 cm^3, resulting in an active volume of 20% of the total volume.

The requirements for turbocompressors, not only such as the Solar Impulse cabin air pressurization system but also the other mentioned applications such as heat pumps and fuel-cell compressors, demand low flow rates (e.g., 1–20 g/s) at relatively high pressure ratios (e.g., 1.3 to 3). The characteristic parameter's volume flow $\dot{V}$ (in cubic meter per second), ideal specific work $h_{t,s}$ (in Joule per kilogram), and angular velocity ω (in radian per second) can be compiled in the nondimensional parameter specific speed ω_s, i.e.,

$$\omega_s = 2\frac{\phi_{t1}^{1/2}}{\psi_s^{3/4}} = \omega\frac{\dot{V}_{t1}^{1/2}}{\Delta h_{t,s}^{3/4}}. \tag{3}$$

This parameter is composed of the flow coefficient, i.e.,

$$\phi_{t1} = \frac{\dot{V}_{t1}}{d_2^2 u_2} \tag{4}$$

(where u_2 is the circumferential speed at radius $d_2/2$) and the isentropic head-rise coefficient, i.e.,

$$\psi_s = \frac{\Delta h_{t,s}}{u_2^2} \tag{5}$$

and therefore, it is also clearly nondimensional. The downscaling of a macro turbomachine for constant specific speed and lower volume flow therefore leads to an increase in rotational speed.

The power density in electrical machines scales with speed, i.e.,

$$\frac{P}{V} \propto n. \tag{6}$$

Therefore, the overall volume of the electrical machines in the example above is also 1/4 of the original one.

In contrast with that of the electrical machines, the size of the power electronics mainly scales with the power rating and is minimized by choosing the correct topology through efficiency improvements and the use of high switching frequencies in order to reduce the volume of passive components. For systems with high power ratings, the size of the control electronics is negligible compared with that of the power electronics. However, for ultrahigh-speed machines with low power ratings (e.g., 100 W), the control-electronics size becomes significant. Generally, the size of the control electronics scales with the complexity of the control method selected, and the complexity depends on the topology and the modulation schemes used.

III. Electrical Machine

The challenges in the machine design are the mechanical rotor design, particularly the stresses in the PM, and the

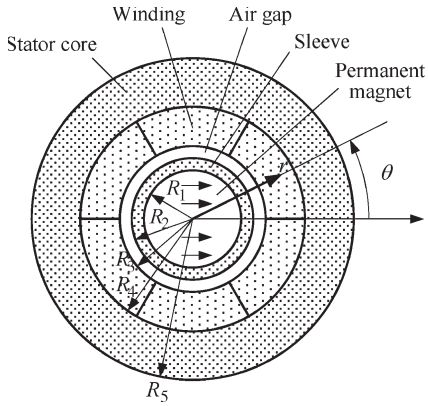

Fig. 2. Machine cross section. Diametrically magnetized cylindrical PM rotor inside a slotless stator.

minimization of high-frequency losses due to eddy currents in copper, iron, and air friction.

The PM machine has been optimized for the lowest losses regarding several constraints, e.g., maximal active length, maximal iron diameter, minimal sleeve thickness, minimal air gap, etc. For this reason, an optimization method has been developed, which takes air-friction losses, iron losses, copper losses, and eddy-current losses into account [9]. The machine has been optimized for a rated power of 150 W, which results from the thermodynamic design for an inlet temperature of 220 K and a pressure ratio of 2.25 at an inlet pressure of 444 kPa. However, under laboratory conditions, the inlet temperature is 300 K, and therefore, the required power is 350 W, which leads to higher ohmic losses in the windings (34.4 W at laboratory conditions compared with 6.8 W at rated conditions). The thermal design has been therefore done for laboratory conditions (see Section VI).

The rotor of the PM motor consists of a diametrically magnetized, not segmented cylindrical, SmCo PM encased in a retaining titanium sleeve ensuring sufficiently low mechanical stresses on the magnet (cf., Fig. 2). The eccentricity is minimized by shrink-fitting the sleeve onto the PM and grinding the rotor.

The PM generator utilizes two high-speed ball bearings due to its simplicity and small size (inner diameter: 3.175 mm; outer diameter: 6.35 mm; $l = 2.8$ mm). The ball bearings are assembled at each end of the rotor in order to be able to change them without the need for disassembling the impellers.

The stator magnetic field rotates with a high frequency (8.3 kHz); it is therefore necessary to minimize the losses in the stator core by using amorphous iron and the eddy-current losses in the skewed air-gap winding by using litz wire. The optimization of the machine dimensions shows that air-friction losses influence the optimum design considerably, leading to a small rotor diameter and, therefore, reduced air-friction losses but slightly increased copper losses. Despite the high-speed operation, the machine efficiency at the rated power is 90%, including air-friction and ball-bearing losses.

Due to the low armature reaction of this machine type, the rotor losses can be omitted [10]. The flux densities in the air gap and the iron core are 0.4 T and 1.05 T, respectively. A detailed description of the machine design has been presented in [11], while the optimization process has been presented in [9]. In Tables I and II, the calculated machine data and the calculated machine losses are summarized, respectively. As shown in [11], the loss calculations are in good agreement with the measurement for this motor type.

TABLE I
ELECTRICAL-MACHINE DATA

Description	Value	Unit
Rated speed	500 000	rpm
Rated electric power		
inlet temperature 220 K	150	W
inlet temperature 300 K	350	W
Rated torque	2.86	mNm
Rated machine temperature	120	°C
Magnet flux linkage	0.265	mVs
Back emf at rated speed	13.9	V
Stator inductance	3.3	µH
Stator resistance	0.12	Ω

TABLE II
CALCULATED ELECTRICAL-MACHINE LOSSES

Description	Value	Unit
Copper losses		
Inlet temperature 220 K	6.8	W
Inlet temperature 300 K	34.4	W
Iron losses	0.7	W
Air friction losses	5	W
Bearing losses	5	W
Total losses (with bearing)		
Inlet temperature 220 K	17.5	W
Inlet temperature 300 K	45.1	W
Machine efficiency (low pressure)		
Inlet temperature 220 K	88.3	%
Inlet temperature 300 K	87.1	%

Considering the rated torque and the rotor inertia, the maximal acceleration (dn/dt) is 1 000 000 r/min/s. However, the dynamic performance of the speed controller has been limited to 40 000 r/min/s in order to prevent additional friction in the ball bearings.

IV. INVERTER

The bidirectional pulse-amplitude modulation (PAM) inverter consists of a standard three-phase inverter, an additional buck converter, and a DSP-based control system. The inverter part is controlled in a six-step or block commutation mode, which means that each switch is conducting for 120° electrical degrees, and is therefore switched with the fundamental frequency of the machine. The phase currents are controlled via the buck converter. The dc is measured for the torque controller, whereas the stator voltages are measured for the sensorless rotor position detection and for the speed controller. Using a sensorless rotor positioning technique eliminates the disadvantages of rotor position sensors, such as an increased failure probability and an axial extension of the rotor. Particularly, a longer rotor is unwanted in this application because the critical speeds are lowered. For an inverter with block commutation, the back electromotive force (EMF) can be directly measured during 60° electrical degrees of intervals in each phase.

The power electronics (buck converter and three-phase inverter) has measured efficiencies of 90% at a rated power of 150 W and 82% at 350 W, respectively. At the rated power,

TABLE III
POWER ELECTRONICS

Description	Value	Unit
Rated power	150	W
Measured efficiency (Buck-converter and three phase inverter)	90	%
Dimensions power electronics (b *x* l *x* h)	80 *x* 80 *x* 47	mm
Total weight (electronic)	220	g

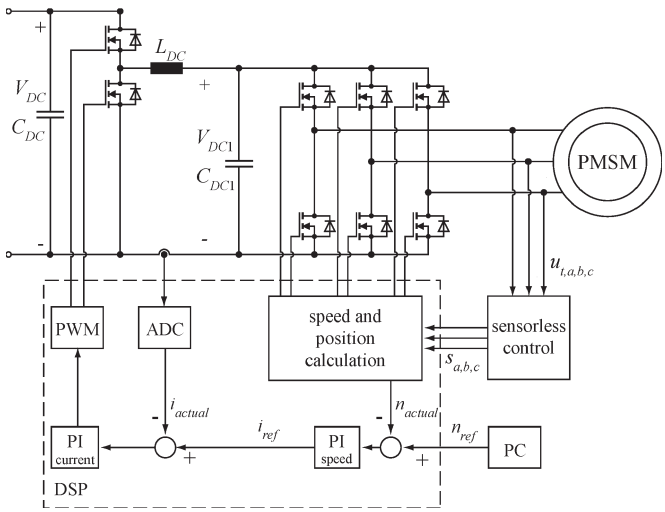

Fig. 3. PAM power electronics and control system for driving an ultrahigh-speed PM machine.

only passive cooling is necessary; however, under laboratory conditions, a higher output power of 350 W is required, and therefore, forced cooling is used at this operating point. In Table III, a summary of important data is shown, while the block diagram of the inverter and the control system is depicted in Fig. 3.

Due to the sinusoidal back EMF, only the fundamental current waveform contributes to the average torque generation. The instantaneous torque can be calculated as (with $L_d = L_q$)

$$T_e = \frac{3}{2} i_q \psi_{\mathrm{pm}} = \frac{3\sqrt{3}}{\pi} i_{\mathrm{dc}} \psi_{\mathrm{pm}} \tag{7}$$

where T_e is the resulting torque, ψ_{pm} is the magnet flux linkage, i_q is the current orthogonal to the direction of the rotor flux linkage (reference frame fixed to the rotor), and i_{dc} is the dc in the buck inductor L_{dc} (cf., Fig. 3). The nonsinusoidal phase currents produce a torque ripple. However, for most of the applications, this torque ripple is negligible due to the high inertia, as compared with the torque ripple variation, which only leads to a very small speed ripple when inertia J is sufficiently high. This relation can be computed as

$$J \frac{d\omega}{dt} = T_e - T_b \tag{8}$$

where T_b is the breaking torque. The usual problem of noise and vibration due to a high torque ripple is outweighed by the noise and the vibration of the turbocompressor.

TABLE IV
TURBOMACHINERY DATA

Description	Value	Unit
Rated speed	500 000	rpm
Rated pressure ratio	2.25	-
Rated mass flow	1	g/s
Rotor inertia	$26 \cdot 10^{-9}$	kgm^2
Compressor efficiency	74	%
Turbocompressor length	80	mm
Turbocompressor diameter	35	mm
Total weight	140	g

V. TURBOMACHINERY

A radial compressor was chosen because this type of compressors can generate high pressure ratios at low mass flows with a single stage. However, to achieve the design goal for a pressure ratio of 2.25 at a very low mass flow of 1 g/s, a two-stage design is employed. The biggest challenge is the manufacturing of the impeller and the fitting between the different pieces, particularly between the impeller and the casing. This is because the manufacturing tolerances cannot be decreased proportional with the downscaling, and therefore, the leakage losses become more dominant for small compressors. This means that the chosen tip clearance (100 μm) is rather high. For a further investigation of the influence of the tip clearance, the clearance of the first stage can be adjusted between 0 and 100 μm.

The first impeller consists of 12 blades (no splitter blades) and has a mean streamline diameter at the inlet of 5.28 mm, while the outlet diameter is 10.5 mm. The second impeller consists of 12 blades and additional splitter blades and has a slightly smaller mean streamline, while the outlet diameter remains the same. After the flow leaves the second stage, it enters the vaneless diffuser and then gets collected in a volute and thereby guided into the exit flange.

The two compressor stages are directly mounted with a shrink fit onto the motor rotor shaft, as shown in Fig. 7. Between the two stages, a spacer sleeve is mounted, and the back-bearing seat is shrink-fitted onto the rotor.

According to the results from the one-stage turbocompressor [8], the design pressure ratio is 2.25 at a mass flow of 1 g/s, which is calculated to be achieved at a rotational speed of 500 000 r/min. The power consumption is depending on the mass flow and the inlet temperature of the air; at the design operating point, it is 350 W under laboratory conditions. The compressor data are compiled in Table IV.

VI. SYSTEM INTEGRATION

Besides the design of the individual components, an analysis of the mechanical stresses and rotordynamics of the common rotor of the electrical machine and the turbomachine, and a thermal design of the entire system are needed. The bending modes of the rotor are depicted in Fig. 4. The length of the shaft is adjusted such that the rated speed falls between the second and third bending modes. In order to reduce losses and to have enough space for the flow director after the first stage, the spacing between the two stages should be as big as possible. However, the third bending mode, which limits

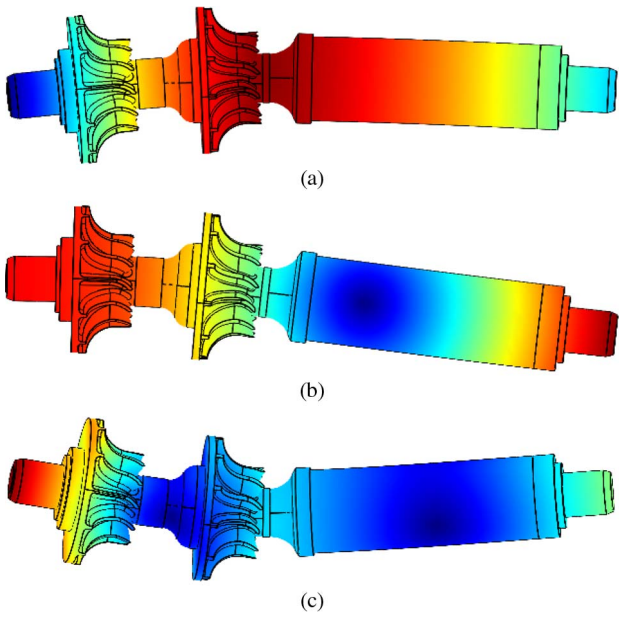

Fig. 4. Bending modes of the two-stage miniature turbocompressor rotor. (a) First bending mode at 2.6 kHz, 156 000 r/min; (b) second bending mode at 5.9 kHz, 354 000 r/min; and (c) third bending mode at 12 kHz, 720 000 r/min. (Blue) No displacement. (Red) Maximal displacement.

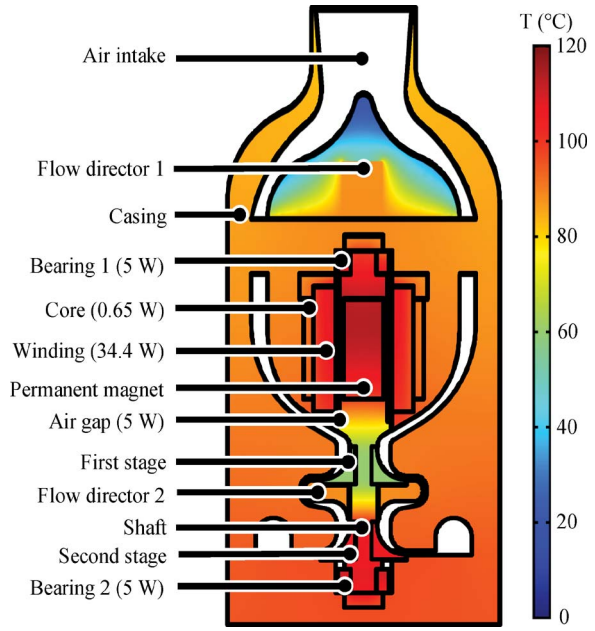

Fig. 5. FE simulations of the temperature distribution under laboratory conditions, at 500 000 r/min, and a drive power of 350 W, assuming an inlet temperature of 300 K.

the maximum speed, is reduced with an increase in the rotor length. Therefore, the space between the two stages is limited. The bending modes' calculations have been made during the machine optimization process with an analytical approach in order to define geometric constraints for the machine. The final rotordynamic design has been verified with 3-D finite-element (FE) simulations. Furthermore, the torsional vibration modes are much higher than the bending modes and have not been therefore added to the rotordynamic analysis.

The main cooling of the motor and the bearings is due to the airflow; the input air first circulates around the motor and bearing 1 and thereby cools them. Because of this special design, no additional cooling fins are needed to guarantee a safe operation under laboratory conditions. The most critical spot is ball bearing 2, which produces high losses and has worse cooling conditions than bearing 1. The maximal allowed temperature in the bearings is 200 °C. A thermal FE analysis of the integrated system under laboratory conditions, including the calculated losses, can be found in the cross-sectional view in Fig. 5. It can be seen that the temperatures in ball bearing 2 do not exceed 110 °C.

VII. Test Bench Setup

An experimental test bench is built in order to verify theoretical considerations and the feasibility of such ultra-compact ultrahigh-speed electrically driven turbocompressor systems (see Fig. 6). Therefore, two valves are connected to the compressor inlet and outlet, respectively, for setting the input and output pressure conditions. When the first valve is fully open, the second valve acts as a variable load, and therefore, measurements in the overpressure condition can be performed. For low-pressure conditions, the second valve is open, and the input pressure is adjusted using the first valve.

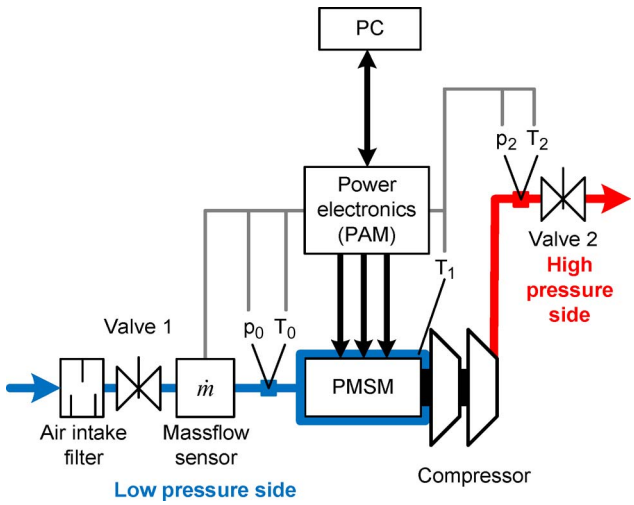

Fig. 6. Test bench setup including mass flow sensor, two valves (for overpressure and low pressure), and two thermocouples for temperature monitoring.

A pressure sensor and a thermocouple are placed between the compressor output and the valve. At the compressor inlet, a pressure sensor, a thermocouple, and a mass flow sensor are used (see Fig. 7). Additionally, two thermocouples are used to monitor the power-electronic and motor-winding temperatures. Due to the fact that the motor is of synchronous type, the speed does not have to be measured separately. All measured data are collected by the DSP-based control system and is transmitted to a personal computer for online and offline analyses.

VIII. Measurements

First, the compressor map depicting the pressure ratio versus the mass flow for different rotational speeds is measured.

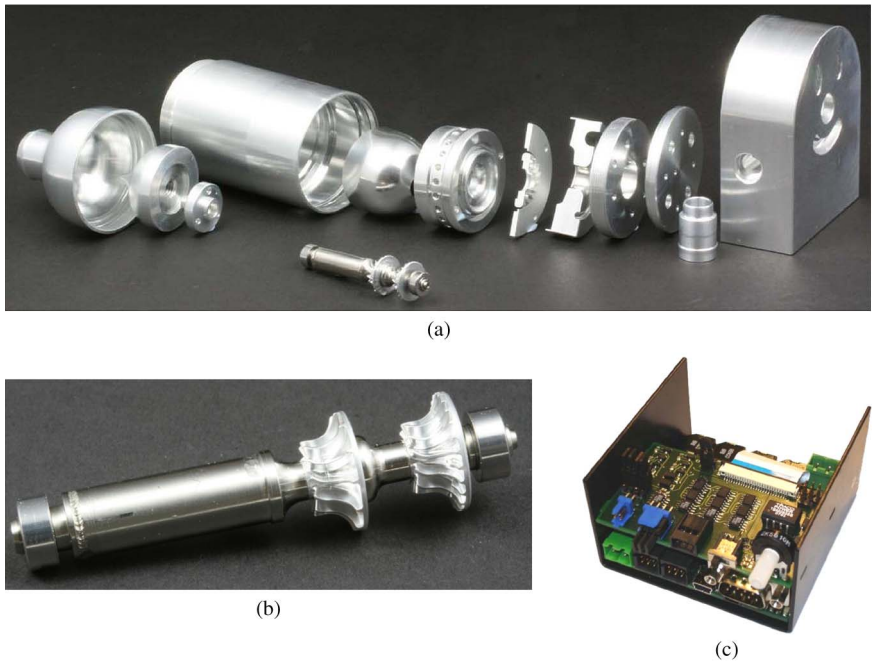

Fig. 7. Miscellaneous components of (a) the miniature two-stage electrically driven compressor, (b) the assembled miniature two-stage rotor, and (c) the power and control electronics including the measurements of mass flow, pressure, and temperature (80 mm × 80 mm × 47 mm).

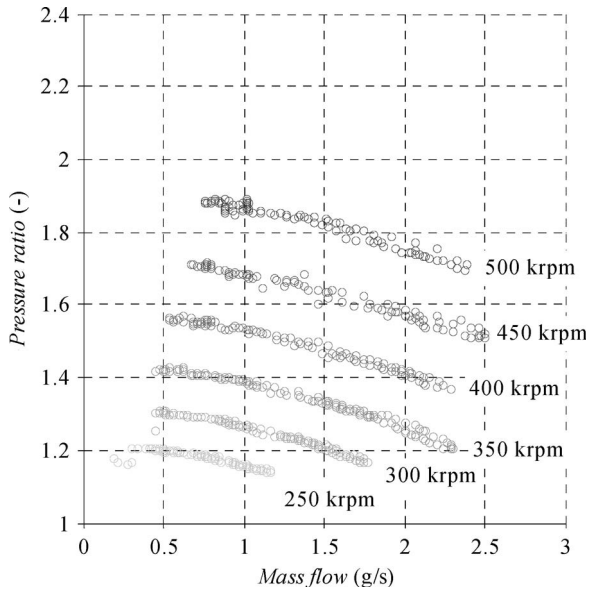

Fig. 8. Measured overpressure compressor map of the miniature turbocompressor, with a clearance of 35 μm at the first compressor wheel.

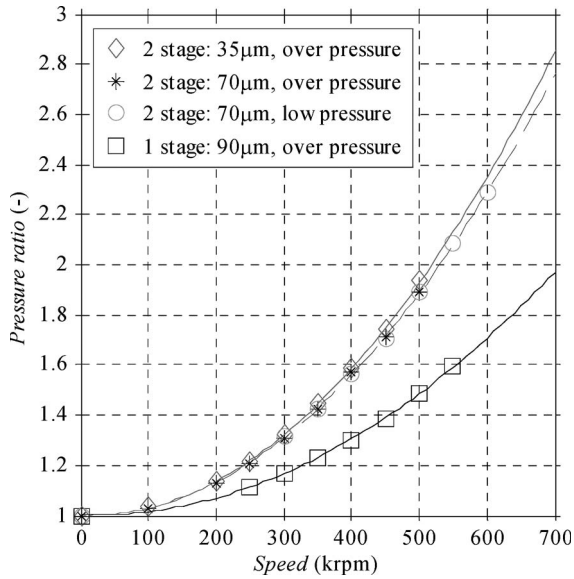

Fig. 9. Measurements and interpolation of maximal pressure ratio for overpressure and low-pressure conditions, and for 70- and 35-μm clearance. (Green dashed line) the maximal pressure ratio for the one-stage compressor for a clearance of approximately 90 μm.

Two different tip clearances are tested (35 and 70 μm), and both overpressure and low-pressure conditions are verified. In Fig. 8, it can be seen that, at a rated speed of 500 000 r/min, a pressure ratio of 1.95 is achieved with a tip clearance of 35 μm, whereas the maximal pressure ratio drops to 1.9 with a tip clearance of 70 μm (see Figs. 9 and 10). This is lower than the prediction of 2.25. One main factor for this difference is the mechanical tolerances in the manufacturing, which are not sufficiently small yet and result in the leakage and the secondary airflow. Moreover, the two-stage design needs a flow director with small radii between the two stages, which leads to an additional pressure drop, compared with the one-stage turbocompressor system [8]. In Fig. 11, the electric-power consumption of the turbocompressor system is shown.

In Fig. 9, the maximal pressure ratios of the one- and two-stage compressors are compiled. It can be seen that the predicted pressure ratio of 2.25 of the two-stage compressor is reached at a speed of 600 000 r/min, whereas the one-stage compressor would reach this ratio at 800 000 r/min, which is clearly too high for ball bearings.

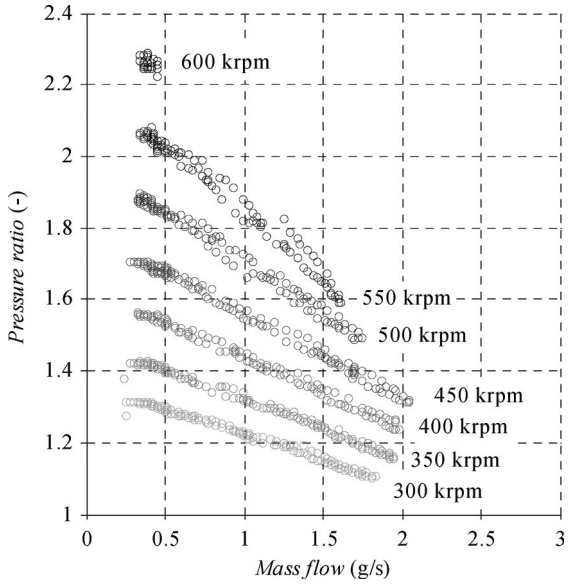

Fig. 10. Measured low pressure compressor map of the miniature turbocompressor, with a clearance of 70 μm at the first compressor wheel.

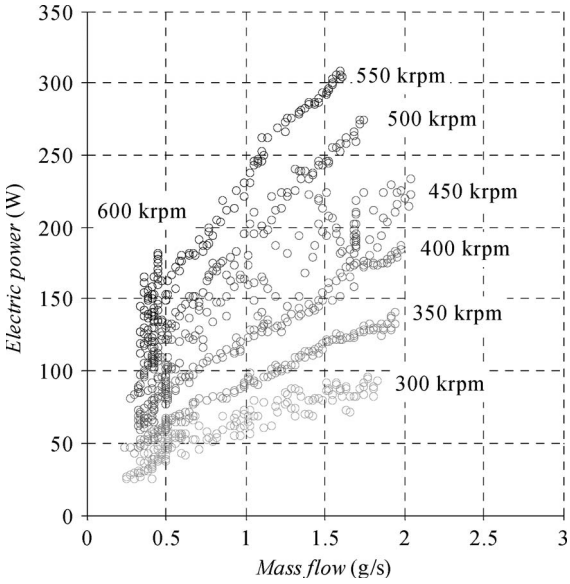

Fig. 11. Measured electric power consumed by the high-speed electric drive system of the miniature turbocompressor at low-pressure conditions.

The compressor efficiency can be calculated from the measured pressure ratio and the input and output air temperatures with

$$\eta_i = \frac{T_1\left[\left(\frac{p_2}{p_1}\right)^{\frac{\kappa-1}{\kappa}} - 1\right]}{T_2 - T_1} \tag{9}$$

where κ is the adiabatic exponent. The input air temperature measurement is located directly before the first compressor stage in order not to include the air heating by the motor. Due to the compact design, it is not possible to measure the temperature between the first and second stages; therefore, no individual stage efficiencies can be measured.

The measured efficiency at the operating point (500 000 r/min and 1 g/s) is 60%. This is lower than the calculated efficiency of 74% due to the same reasons as for the difference in measured and calculated pressure ratios and can be increased by decreasing the tip clearance or a redesign of the second flow director or the impellers.

IX. Conclusion

This paper has presented the design of a miniature 500 000-r/min electrically driven turbocompressor for various applications in the area of air and gas pressurizations for future automotive, aerospace, and residential applications with a strong link to renewable-energy systems. The system design is based on an electrical drive system achieving the highest rotational speeds. The manufacturing of miniaturized compressors represents difficulties due to smallest contours and desirably small tolerances. However, measurements have shown that, despite these difficulties, the system has a performance close to the specified design operating point, and turbocompressors with speeds even above 500 000 r/min are feasible.

This new system have fulfilled the specification regarding the mass flow and the rotational speed, but it does not achieve the necessary pressure ratio yet. The next step in the project will be to decrease the clearances between the compressor stages and the casing, as well as between the second flow director and the rotor further. In the second step, a redesign of the compressor wheels will be undertaken.

Bearing lifetime is the main challenge before such ultrahigh-speed electrically driven compressors can be widely used in industry. For reaching acceptable lifetime and oil-free compressor systems, the high-speed ball bearings must be replaced by air bearings or magnetic bearings.

References

[1] N. Lapeña-Rey, J. Mosquera, E. Bataller, and F. Ortí, "The boeing fuel cell demonstrator airplane," presented at the AeroTech Congr. Exhib., Los Angeles, CA, Sep. 2007, p. 2007-01-3906.

[2] H. T. Bradley, A. B. Moffitt, W. R. Thomas, D. Mavris, and E. D. Parekh, "Test results for a fuel cell-powered demonstration aircraft," presented at the Proc. Power Systems Conf., New Orleans, LA, Nov. 2006, p. 2006-01-3092.

[3] B. Blunier and A. Miraoui, "Air management in PEM fuel cell: State-of-the-art and prospectives," in *Proc. Int. Aegean Conf. Elect. Mach. Power Electron., Electromotion*, Bodrum, Turkey, Sep. 10–12, 2007, pp. 245–254.

[4] J. Schiffmann, "Integrated design, optimization and experimental investigation of a direct driven turbocompressor for domestic heat pumps," Ph.D. dissertation, Ecole Polytechnique Federale de Lausanne, Lausanne, Switzerland, 2008.

[5] S. Kang, S.-J. J Lee, and F. B. Prinz, "Size does matter, the pros and cons of miniaturization," *ABB Rev.*, vol. 2, pp. 54–62, 2001.

[6] A. Binder and T. Schneider, "High-speed inverter-fed AC drives," in *Proc. Int. Aegean Conf. Elect. Mach. Power Electron., Electromotion*, Bodrum, Turkey, Sep. 10–12, 2007, pp. 9–16.

[7] [Online]. Available: www.solarimpulse.com

[8] C. Zwyssig, D. Krähenbühl, H. Weser, and J. W. Kolar, "A miniature turbocompressor system," in *Proc. SES*, Zurich, Switzerland, Sep. 8–10, 2008, pp. 144–148.

[9] J. Luomi, C. Zwyssig, A. Looser, and J. W. Kolar, "Efficiency optimization of a 100-W 500 000-r/min permanent-magnet machine including air-friction losses," *IEEE Trans. Ind. Appl.*, vol. 45, no. 4, pp. 1368–1377, Jul./Aug. 2009.

[10] C. Zwyssig, S. D. Round, and J. W. Kolar, "Analytical and experimental investigation of a low torque, ultra-high speed drive system," in *Conf. Rec. 41st IEEE IAS Annu. Meeting*, 2006, vol. 3, pp. 1507–1513.

[11] C. Zwyssig and J. W. Kolar, "Design considerations and experimental results of a 100 W, 500 000 rpm electrical generator," *J. Micromech. Microeng.*, vol. 16, no. 9, pp. 297–302, Sep. 2006.

Daniel Krähenbühl (S'08) received the M.Sc. degree in electrical engineering from the Swiss Federal Institute of Technology (ETH) Zurich, Zurich, Switzerland, in 2007, where he is working toward the Ph.D. degree in the Power Electronic Systems Laboratory, focusing on ultrahigh-speed electrically driven turbocompressors and turbine generator systems.

His focus during his studies has been on mechatronics, power electronics, and microelectronics. In 2007, he concluded his M.Sc. thesis in which he designed and realized a 1.5-kW converter for bearingless motors, in cooperation with Levitronix GmbH. Since June 2010, he has been with Celeroton Ltd., Zurich, a spin-off company in the area of high-speed electrical drive systems.

Christof Zwyssig (M'10) received the M.Sc. and Ph.D. degrees in electrical engineering from the Swiss Federal Institute of Technology (ETH) Zurich, Zurich, Switzerland, in 2004 and 2008, respectively.

He studied power electronics, machines, and magnetic bearings and was engaged in research on high-speed electrical drive systems and their power electronics. He was also with the Chalmers University of Technology, Gothenburg, Sweden, where he was involved in the field of wind turbines. Since January 2009, he has been with Celeroton Ltd., Zurich, a spin-off company in the area of high-speed electrical drive systems, of which he is a co-founder.

Hansjörg Weser received the Dr.Eng. degree in turbomachinery (turbines, compressors, and pumps) from Dresden University of Technology, Dresden, Germany.

He has worked for several companies. He gained experience as the Development Manager for a German plant manufacturer, where he was responsible for the development of turbo expanders for air separation plants, as well as for a variety of special turbocompressor developments. In the early 1990s, he became the Director of the technical department for a manufacturer of cryopumps in Switzerland. Since the mid-2000s, he has been the General Manager of High-Speed Turbomaschinen GmbH, Lehre, Germany, of which he is a co-founder.

Johann W. Kolar (SM'04–F'10) received the M.Sc. and Ph.D. degrees (*summa cum laude/promotio sub auspiciis praesidentis rei publicae*) from Vienna University of Technology, Vienna, Austria.

Since 1984, he has been an Independent International Consultant in close collaboration with the Vienna University of Technology in the fields of power electronics, industrial electronics, and high-performance drives. He has proposed numerous novel pulsewidth-modulation converter topologies and modulation and control concepts, e.g., the VIENNA Rectifier and the three-phase ac–ac sparse matrix converter. He has published over 350 scientific papers in international journals and conference proceedings and is the holder of 75 patents. On February 1, 2001, he was appointed Professor and Head of the Power Electronic Systems Laboratory, Swiss Federal Institute of Technology (ETH) Zurich, Zurich, Switzerland. He initiated and/or is the founder/cofounder of four spin-off companies targeting ultrahigh-speed drives, multidomain/level simulation, ultracompact/ultraefficient converter systems, and pulsed-power/electronic-energy processing. The focus of his current research is on ac–ac and ac–dc converter topologies with low effects on the mains, e.g., for power supply of data centers and more-electric-aircraft and distributed renewable-energy systems. His other research interests are the realization of ultracompact and ultraefficient converter modules employing latest power semiconductor technology (e.g., SiC), novel concepts for cooling and electromagnetic-interference filtering, multidomain/scale modeling/simulation and multiobjective optimization, physical model-based lifetime prediction, pulsed power, and ultrahigh-speed and bearingless motors.

Dr. Kolar is a member of the Institute of Electrical Engineers of Japan (IEEJ) and of international steering committees and technical program committees of numerous international conferences in the field (e.g., Director of the Power Quality Branch of the International Conference on Power Conversion and Intelligent Motion). He is the founding Chairman of the IEEE Power Electronics Society Austria and Switzerland Chapter and Chairman of the Education Chapter of the European Power Electronics and Drives Association. From 1997 to 2000, he was an Associate Editor of the IEEE TRANSACTIONS ON INDUSTRIAL ELECTRONICS, and since 2001, he has been an Associate Editor of the IEEE TRANSACTIONS ON POWER ELECTRONICS. Since 2002, he has also been an Associate Editor of the *Journal of Power Electronics* of the Korean Institute of Power Electronics and a Member of the Editorial Advisory Board of the *IEEJ Transactions on Electrical and Electronic Engineering*. He was a recepient of the Erskine Fellowship from the University of Canterbury, New Zealand, in 2003. He was also a recepient of the Best Transactions Paper Award of the IEEE Industrial Electronics Society in 2005, the Best Paper Award of the International Conference on Performance Engineering in 2007, the First Prize Paper Award of the IEEE Industry Applications Society Industrial Power Converter Committee in 2008, and the Annual Conference of the IEEE Industrial Electronics Society Best Paper Award of the Industrial Electronics Society Power Electronics Technical Committee in 2009. In 2006, the European Power Supplies Manufacturers Association named the Power Electronics Systems Laboratory, ETH Zurich, as the leading academic research institution in power electronics in Europe.